Lin-Ding Yuan[1], Xiuwen Zhang[1], Carlos Mera Acosta[2], Alex Zunger[1]

[1]Renewable and Sustainable Energy Institute, University of Colorado, Boulder, Colorado 80309, USA

[2]

Figure S1: Energy spectrum of antiferromagnetic tetragonal CuMnAs on the conventional k-paths. a with SOC turned off, and **b** with SOC turned on.

Figure S2 illÜÚÛÙaÛeÚÛhe?hiddeÕÚ×iÕ×ÖlaÙiáaÛiÖÕ?effecÛiÕheßagÖÕalCÖBÙ$_2$ [3] being bulk SST-2 class (MSG C_c2/c) but made of SST-5 class FM $CoBr_2$ layers (-sector and -sector in Fig. S2a). The crystal is antiferromagnetically ordered with its magnetic moments collinearly aligned in (001) direction. The two $FeBr_2$ layers are connected by both the and the symmetry which restores the spin degeneracy of the bulk and results in a compensated net spin polarization (Fig. S2b). However, the corresponding spin polarization for the bottom two conduction bands (C1 and C2) projected onto -sector and -sector (hidden spin polarization), shown in Fig. S2c, are non-zero and compensate each other.

crystal structure of antiferromagnetic $CoBr_2$ composed of two ferromagnetic layers with opposite magnetization (indicated by red and blue polyhedra) in the unit cel lyhedra to red. The crystal and magnetic structure for hexagonal $CoBr_2$ used in our DFT calculations are taken from Ref. [3]. The electronic structure and hidden spin polarization are calculated using the PBE+U method with U=3.32 eV, J=0 eV on Co-3d orbits.

Figure S3 illÜÚÛÙaÛeÚ Ûhe ʔhiddeÕ Ú×iÕ ×ÖlaÙiáaÛiÖÕʔ effecÛ iÕ ÛeÛÙagÖÕal $Ca_3Ru_2O_7$ [4] being bulk SST-3 class (MSG P_cna2_1) but made of SST-5 class FM RuO_7 sectors (-sector and -sector in Fig. S3a). The crystal is antiferromagnetically ordered with its magnetic moments collinearly aligned in (010) direction. The two ferromagnetically ordered Ru_2O_7

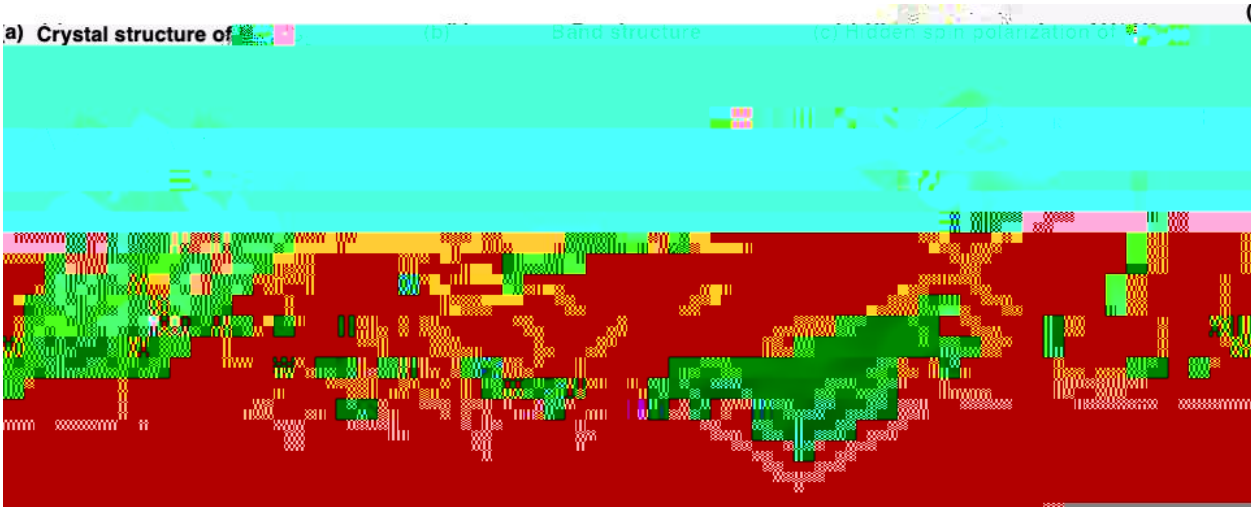

crystal structure of antiferromagnetic MnS_2 composed of two antiferromagnetic sectors with opposite magnetic ordering (indicated by red and blue polyhedra) in the unit cell. The two layers are referred as sector- and sector- , respectively; spin degenerate bands of MnS_2. Hidden spin polarization from each individual sector of the highest two valence bands (V1 and V2) on k-plane. The up and down spins are mapped to the color from blue to red. The crystal and magnetic structure for tetragonal MnS2 used in our DFT calculations are taken from Ref. [6]. The electronic structure and hidden spin polarization are calculated using the PBE+U method with U=5.0 eV, J=0 eV on Mn-3d orbits.

Figure S6 illustrates how SST-4 class monolayers (with SS) are -asymmetric subsets forming an SST-1 class bilayer that is -symmetric (without SS), i.e., spin polarization at different SST-4 class sectors is mutually compensated by means of the stacking of layers that restores the symmetry. The DFT band structure calculations for the SST-4 class FeSe monolayer reveals a spin splitting of about 5 meV near the Fermi energy (Fig. S6a). This spin splitting is the result of the antiferromagnetic configuration with two different local environments in the unit cell (dotted line) breaking the and symmetries. When FeSe monolayers interact via the Van der Waals potential to form a bilayer with layer exactly equivalent (i.e., connected through the symmetry), the FeSe bilayer belongs to the SST-1 class. As a consequence, the band structure is completely spin degenerated (Fig. S6b). The compensation between FeSe layers in the bilayer system explicitly demonstrates the concept of the hidden AFM-SS. Remarkable, the bands in the -symmetric bilayer have hidden spin-polarization, where spin bands are formed by orbitals spatially localized at different -asymmetric subsets (Fig. S6b). As expected, an external electric field breaks the symmetry, leading then to manifestation of the hidden spin polarization in a bilayer with -asymmetric subsets that compensate each other. The SS magnitude depends on the intensity of the external electric field. Different from the relativistic Rashba and Dresselhaus SS that require the SOC, the electric field induces in the SST-1 FeSe bilayer a non-zero SS even in the absence of SOC (Fig. S6c).